# Supplementary Information

## Nanoparticle-Decorated Bismuth/Nickel Doped $Sr_2Fe_{1.5}Mo_{0.5}O_{6-\delta}$ Cathode for Enhanced $CO_2$ Reduction in Solid Oxide Electrolysis Cells

Mohammadali Emadi, Eric Croiset *

*Department of Chemical Engineering, University of Waterloo,*

*Waterloo, Ontario, N2L 3G1, Canada*

*E-Mail addresses: smemadif@uwaterloo.ca (M. Emadi),*

*ecroiset@uwaterloo.ca (E. Croiset)*

* *Corresponding author.*

## Contents

## 1. XRD comparison of as-synthesized with reduced and reoxidized samples

XRD was also used to look at three samples of the BiSFMNi material: the as-synthesized (oxidized), reduced, and reoxidized states and the results are shown in Figure S1. This was done to see whether the structure could return to its original state. The XRD analysis of the reoxidized BiSFMNi sample showed that the double perovskite structure had completely recovered. There were no peaks that matched the previously exsolved Fe–Ni alloy or Ruddlesden–Popper phase. This means that the changes in structure caused by reduction is reversible. The reoxidation process effectively puts the exsolved metal species back into the lattice, bringing the material back to its original double perovskite phase.

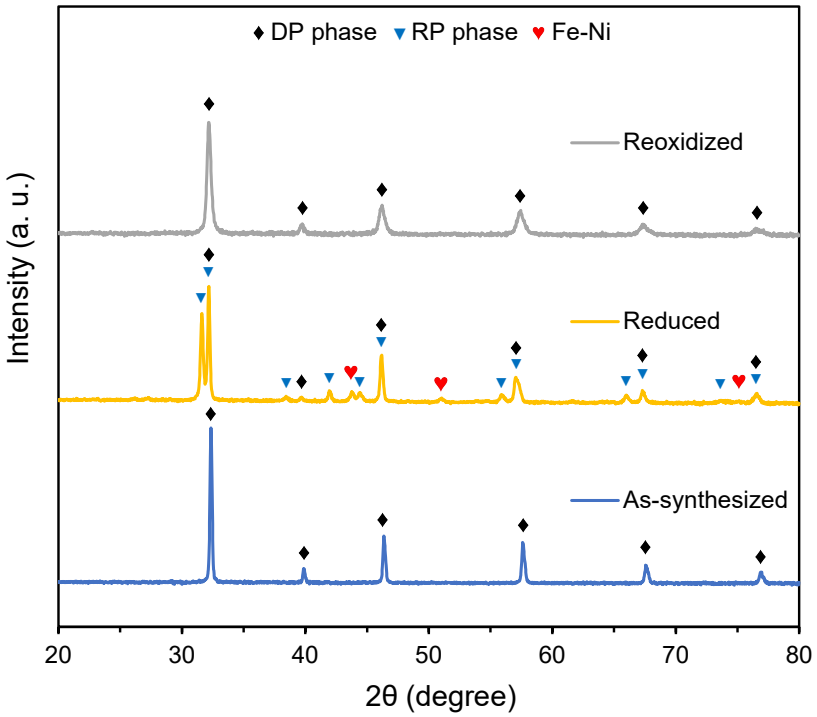


Figure S1. XRD patterns of BiSFMNi in oxidized, reduced, and reoxidized states.

## 2. Stability test of BiSFMNi perovskite in $CO/CO_2$ environments

The chemical stability of BiSFMNi was evaluated under $CO/CO_2$ environments at elevated temperature. Powder and sintered pellet samples were placed in an alumina boat and heated in a tubular furnace to 800 °C (5 °C $min^{-1}$) under a continuous flow of either pure $CO_2$ or 50% $CO/CO_2$ for 24 hr. The exposed powder samples were analyzed by X-ray diffraction to assess bulk phase stability, while the pellets were examined by Raman spectroscopy to identify potential carbon-related species.

Figure S2 presents the XRD and Raman results of BiSFMNi samples after 24 h exposure at 800 °C in $CO_2$ and 50% $CO/CO_2$ mixtures. The XRD patterns show that BiSFMNi retains its double perovskite structure after exposure to both $CO_2$ and $CO/CO_2$ atmospheres, with no major secondary phases detected. Two weak peaks around 25° were observed only under the 50% $CO/CO_2$ atmosphere, which can be attributed to trace $SrCO_3$ formation. This minor carbonate phase likely originates from limited surface reactions between Sr and $CO_2$ during partial reduction but remains negligible in intensity, indicating that the bulk structure remains intact. In addition, Raman spectra of the exposed pellets showed no D (~1340 $cm^{-1}$) or G (~1580 $cm^{-1}$) bands associated with carbon species, confirming the absence of carbon deposition. These complementary results demonstrate that BiSFMNi exhibits excellent structural and chemical stability in $CO/CO_2$ atmospheres and high carbon tolerance, confirming its suitability as a durable SOEC cathode material.

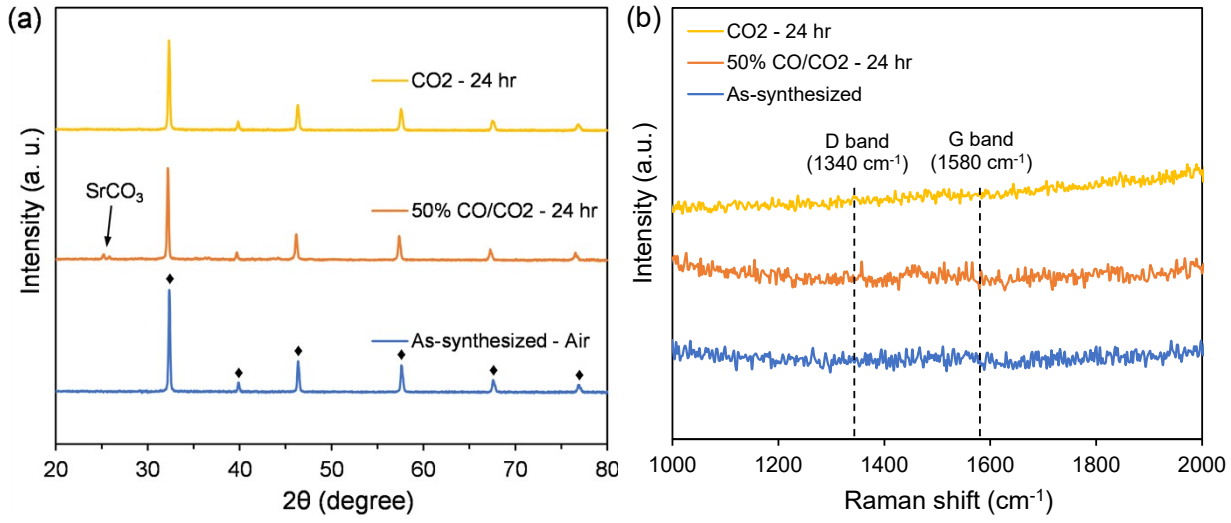


Figure S2. (a) XRD patterns and (b) Raman spectra of BiSFMNi in as-synthesized state and after CO/Co environment treatments at 800 °C.

## 3. Thermal stability

The Thermogravimetric analysis (TGA) results, shown in Figure S3, provide valuable insights into the thermal stability and oxygen release behavior of the perovskite powders under different atmospheres. Both SFM and BiSFMNi samples exhibit gradual weight loss with increasing temperature, mainly associated with lattice oxygen release and minor surface species desorption such as adsorbed water and carbonates. The TGA curves can be divided into three distinct weight-loss regions: (i) 25–400 °C, corresponding to desorption of adsorbed water and surface species, (ii) 400–800 °C, associated with lattice oxygen release and redox activity of the perovskite, and (iii) above 800 °C, linked to deep oxygen loss and potential partial structural instability. In air, the weight loss is minimal compared to inert ($N_2$) or reactive ($CO_2$) conditions, confirming the higher stability of the perovskite lattice in oxidizing environments. Under pure $CO_2$, both SFM and BiSFMNi exhibit slightly higher weight loss, which may be related to surface interactions with $CO_2$ or transient carbonate formation and decomposition. Notably, the Bi and Ni doping shows improved thermal stability compared to pristine SFM, with less overall weight change across all atmospheres, suggesting that co-doping helps stabilize the oxygen sublattice and suppresses excessive oxygen release.

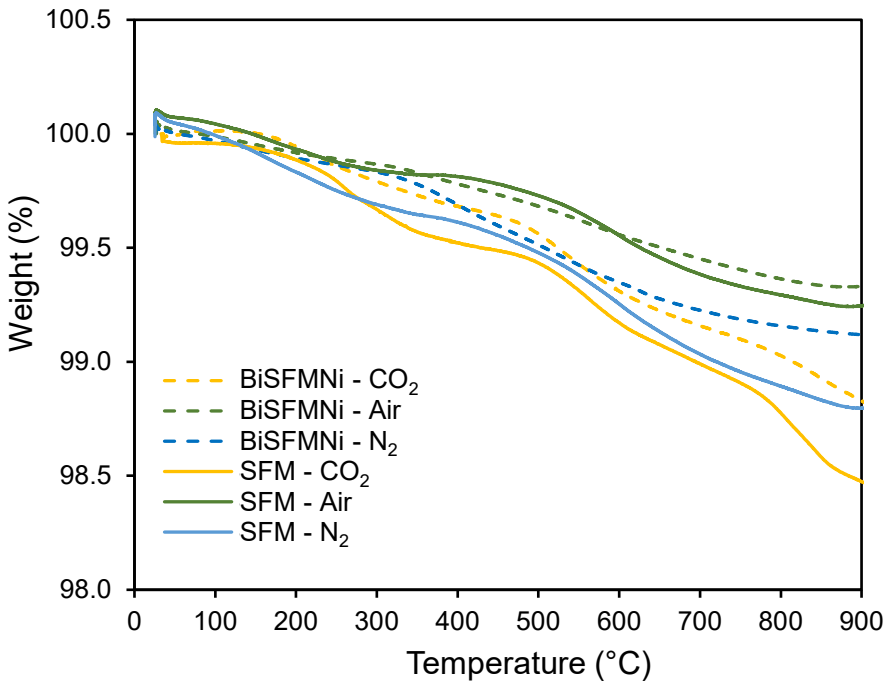


Figure S3. TGA of SFM and BiSFMNi samples in $N_2$, Air and $CO_2$ atmospheres.

## 4. TEM analysis

The exsolution behavior and structural evolution of the BiSFMNi were investigated using transmission electron microscopy techniques. Figure S4 and S5 present comparative TEM images of the sample before and after reduction at 800 °C for 2 hours in 5% $H_2$/Ar atmosphere.

In the as-synthesized state (Figure S4), the perovskite exhibits a cubic, dense surface morphology without any apparent nanoparticle decoration. Energy-dispersive X-ray spectroscopy (EDS) confirms a homogeneous elemental distribution across the sample. The quantified atomic percentages closely match the nominal target composition of $Bi_{0.1}Sr_{1.9}Fe_{1.4}Ni_{0.1}Mo_{0.5}O_{6-\delta}$, verifying the successful synthesis and cation incorporation into the lattice.

After reduction (S5), clear morphological changes are observed. Numerous nanoparticles have emerged and are uniformly distributed on the surface of the perovskite matrix. Scanning transmission electron microscopy (STEM) images clearly show these nanoparticles anchored to the host surface. High-resolution TEM (HR-TEM) images reveal lattice fringes indicating the crystalline nature of both the perovskite matrix and the exsolved nanoparticles. The interface between the nanoparticle and the host lattice appears coherent, suggesting strong integration and good adhesion.

To further analyze the composition and phase separation, EDS analysis carried out at two places: one on a nanoparticle and one on the perovskite bulk. The EDS spectrum from the nanoparticle area had a strong Fe peak and a smaller but clear Ni peak. This means that Fe–Ni alloy nanoparticles were formed, which is what was seen in the XRD as the Fe–Ni phase. However, the EDS spectra from the perovskite bulk showed Sr, Fe, Mo, Bi, O, and a very little quantity of Ni. This means that most of the Ni ions were exsolved during reduction, but a small amount stayed in the bulk lattice. Ni exsolution happens over time. It is likely that after a longer reduction time (like 5 hours), almost all of the Ni will be exsolved to form more nanoparticles. This migration of Ni from the lattice to the surface can be harnessed to control the density, size, and distribution of exsolved nanoparticles. The atomic percentages obtained from the EDS analysis after reduction of the bulk perovskite closely match the stoichiometry of the Ruddlesden–Popper phase, $Sr_3Fe_{1.5}Mo_{0.5}O_{6.5-\delta}$, confirming the presence of this secondary phase.

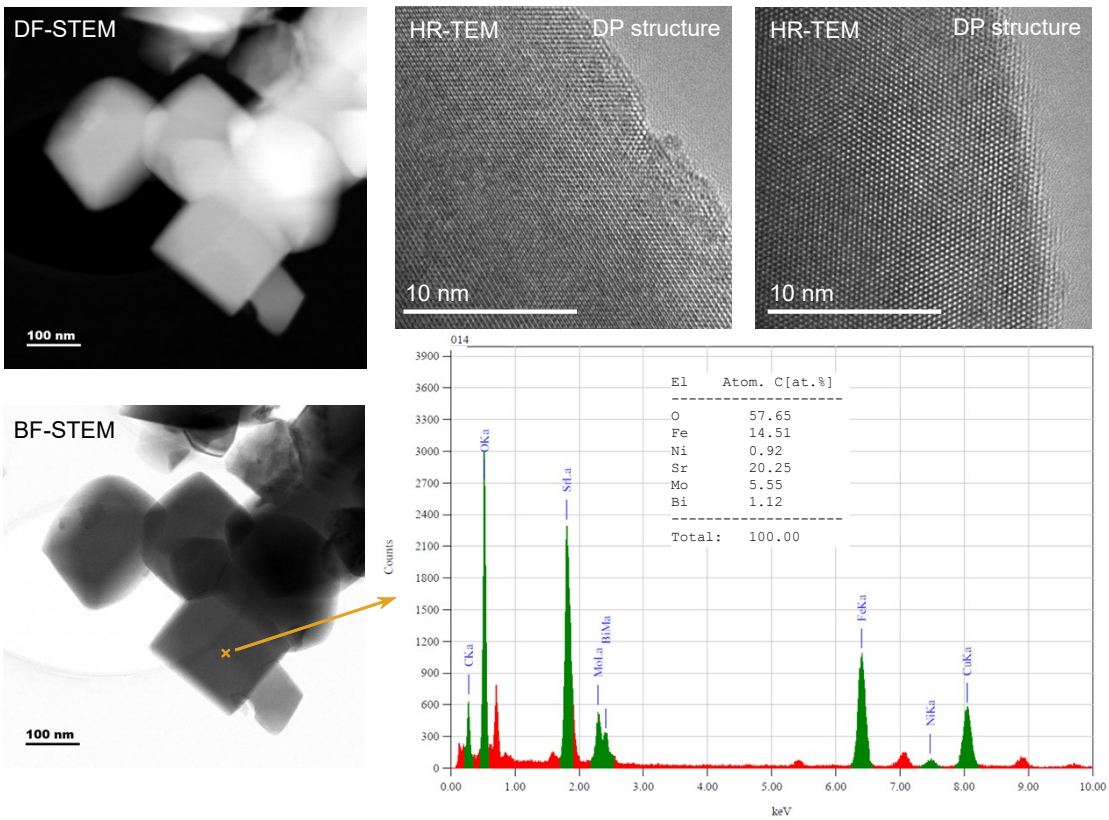


Figure S4. TEM image and EDS analysis of the as-synthesized BiSFMNi sample.

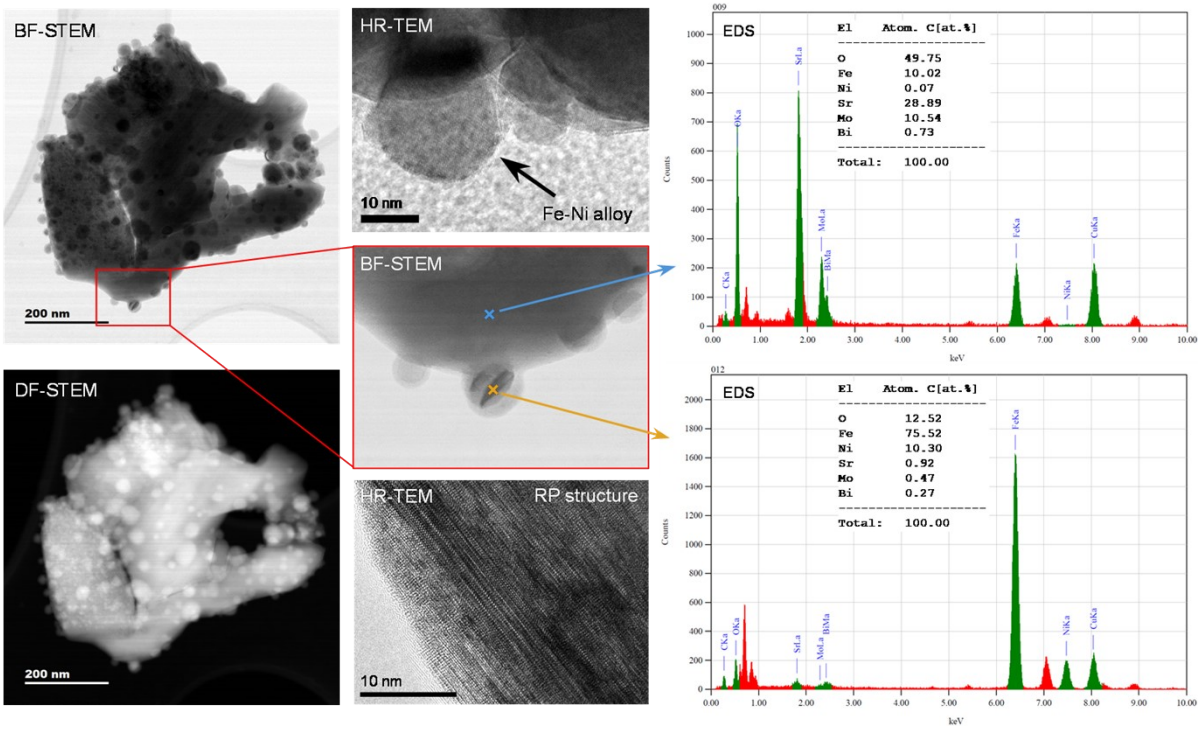


Figure S5. TEM image and EDS analysis of the reduced BiSFMNi sample.

## 5. Cell cross section EDS analysis

Line EDS analysis was performed across to see how the elements were spread out across the cell. In Figure S6, along with the SEM cross-section, the matching elemental intensity profiles are depicted. The figure clearly shows that the layers have different compositions with well-defined interfaces. The LSCF/GDC oxygen electrode has signals for La, Sr, Co, Fe, Gd and Ce, which is expected from its mixed perovskite-fluorite structure. As expected for a LSGM phase, the electrolyte is mostly made up of La, Sr, Ga, and Mg. There is a little area between the electrolyte and the cathode where La and Ce signals are higher than normal. This shows that a thin LDC (La-doped Ceria) buffer layer has been successfully deposited. On the fuel side, the BiSFMNi is confirmed by big signals for Fe, Mo, Bi and a tiny signal for Ni. There was no significant elemental crossover or interdiffusion between neighboring layers, which shows that the spin-coated LDC buffer layer does a good job of keeping the cathode and electrolyte from reacting with one other in ways that are not desirable.

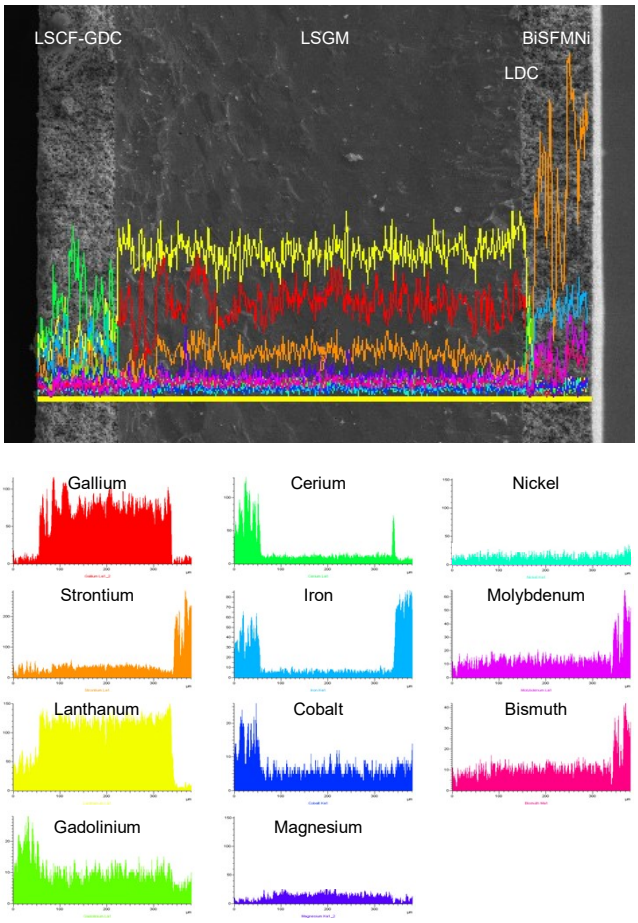


Figure S6. Line EDS elemental mapping across the cell cross-section.

## 6. Thermal expansion analysis

Thermal expansion analysis, presented in Figure S7, shows that the average thermal expansion coefficients (TEC) of SFM and BiSFMNi in the 25–800 °C range are $15.3\times10^{-6}$ $K^{-1}$ and $13.9\times10^{-6}$ $K^{-1}$ respectively. The reduction in TEC upon Bi and Ni incorporation suggests that these dopants decrease lattice expansion. This decrease in thermal expansion enhances the compatibility of the cathode with common solid oxide electrolytes. For reference, LSGM electrolytes exhibit TEC values between $11.4\times10^{-6}$ $K^{-1}$, while La-doped ceria (LDC), as an interlayer, has a TEC of about $13.4\times10^{-6}$ $K^{-1}$. Accordingly, BiSFMNi demonstrates a much better thermal match with both LSGM and LDC compared to undoped SFM, which helps reduce thermal stresses at the cathode-electrolyte interface during high-temperature operation. Moreover, introducing an LDC buffer layer between BiSFMNi and LSGM further mitigates any residual thermal mismatch and improves interfacial stability by accommodating small expansion differences, thus minimizing the risk of cracking or delamination during repeated thermal cycling.

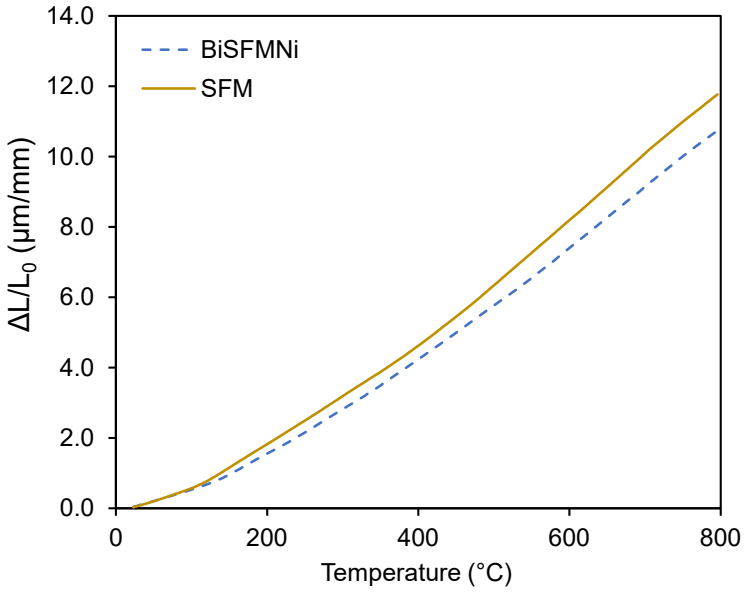


Figure S7. Thermal expansion behavior of the SFM and BiSFMNi samples between 25 °C and 800 °C in air.